Determination of the Structure of ^{31}Ne by a Fully Microscopic Framework

Kosho Minomo,[1] Takenori Sumi,[1] Masaaki Kimura,[2] Kazuyuki Ogata,[3] Yoshifumi R. Shimizu,[1] and Masanobu Yahiro[1]

[1]*Department of Physics, Kyushu University, Fukuoka 812-8581, Japan*
[2]*Creative Research Institution (CRIS), Hokkaido University, Sapporo 001-0021, Japan*
[3]*Research Center of Nuclear Physics (RCNP), Osaka University, Ibaraki 567-0047, Japan*

(Received 31 October 2011; published 31 January 2012)

We perform the first quantitative analysis of the reaction cross sections of $^{28-32}$Ne by ^{12}C at 240 MeV/nucleon, using the double-folding model with the Melbourne g matrix and the deformed projectile density calculated by antisymmetrized molecular dynamics. To describe the tail of the last neutron of ^{31}Ne, we adopt the resonating group method combined with antisymmetrized molecular dynamics. The theoretical prediction excellently reproduces the measured cross sections of $^{28-32}$Ne with no adjustable parameters. The ground state properties of ^{31}Ne, i.e., strong deformation and a halo structure with spin parity $3/2^-$, are clarified.

DOI: 10.1103/PhysRevLett.108.052503 PACS numbers: 21.10.Gv, 21.60.Gx, 24.10.Ht, 25.60.Dz

Introduction.—Exotic properties of nuclei in the ''island of inversion'' fascinate many experimentalists and theoreticians. The term island of inversion was first introduced by Warburton, Becker, and Brown [1] to specify the region of unstable nuclei from ^{30}Ne to ^{34}Mg. According to many experimental and theoretical studies, it turned out that the low excitation energies and the large $B(E2)$ values of the first excited states of nuclei in the island indicate strong deformations [2–7], which eventually cause the *melt* of the neutron shell corresponding to the $N = 20$ magic number (N: neutron number). To understand these features, intruder configurations of the single-particle orbits have been discussed with the shell model [8], the generator coordinate method [9], and the Hartree-Fock (HF) and Hartree-Fock-Bogoliubov methods based on the Skyrme or Gogny interaction [10–13]. In particular, the ^{31}Ne nucleus is very interesting in view of its intruder configurations and a halo structure due to strong deformations. Recently, a systematic investigation employing antisymmetrized molecular dynamics (AMD) with the Gogny D1S interaction has been performed for both even and odd N nuclei in the island of inversion [14]. AMD was shown to give rather large deformations and a small separation energy of the ^{31}Ne as indicated by the preceding studies mentioned above.

Very recently, experimental studies took large steps toward exploring the island of inversion; i.e., the one-neutron removal cross section σ_{-n} of ^{31}Ne at 230 MeV/nucleon was measured by Nakamura *et al.* [15], and the interaction cross section $\sigma_{\rm I}$ of $^{28-32}$Ne by ^{12}C at 240 MeV/nucleon was measured by Takechi *et al.* [16,17]. According to the analysis of the σ_{-n} [15,18–21], the measured large cross section suggested a neutron-halo structure of ^{31}Ne with spin parity $3/2^-$. This conjecture was confirmed by the analysis of the $\sigma_{\rm I}$ [16,17,21], in which neutron configurations with lower partial waves were favored to explain the $\sigma_{\rm I}$ of ^{31}Ne. In Ref. [17], it was shown that s-wave configuration gave slightly better agreement with the data, which implied a possibility of even more drastic change of the nuclear shell structure. Note that $\sigma_{\rm I}$ differs from the total reaction cross section $\sigma_{\rm R}$ by the inelastic cross section(s) due to the excitation of the projectile. For unstable nuclei, however, the two are almost identical, since very few bound excited states exist for such nuclei. Thus, $\sigma_{\rm I}$, as $\sigma_{\rm R}$, can be assumed to represent the *size* of the nucleus.

All aforementioned studies indicate the shell evolution of ^{31}Ne and its halo structure. Quantitative understanding of these properties of ^{31}Ne is, however, still under discussion. This is mainly due to the fact that nuclear many-body wave functions obtained by the high-precision structural models have never been directly applied to reaction calculation. As a first step, in Ref. [22] we analyzed the $\sigma_{\rm I}$ of $^{28-32}$Ne [16,17] with the microscopic double-folding model (DFM) based on the Melbourne g matrix [23]. We adopted the mean-field wave functions based on a deformed Woods-Saxon (WS) potential, with the deformation parameter evaluated by AMD. It was shown that the deformation of the Ne isotopes was indeed important to reproduce the experimental data. The agreement between the calculation and the data was, however, not fully satisfactory. The large difference in $\sigma_{\rm I}$ between ^{30}Ne, ^{31}Ne, and ^{32}Ne could not be explained well, in particular.

In this Letter, we directly incorporate the AMD wave functions of $^{28-32}$Ne in the DFM calculation and see how the structural properties of these nuclei based on AMD are ''observed'' through $\sigma_{\rm I}$. For ^{31}Ne, we further utilize the resonating group method (RGM) to give a proper behavior of the neutron wave function in the tail region. This is the first microscopic calculation of $\sigma_{\rm I}$ for $^{28-32}$Ne with no adjustable parameters. The predicted values of $\sigma_{\rm I}$ are validated by the comparison with the experimental data [16,17]. Through this study, we aim to determine the ground state structure of ^{31}Ne.

Theoretical framework.—We calculate the total reaction cross section σ_R by DFM as in Ref. [22]. This model is accurate, when the projectile breakup is small. This condition is well satisfied for scattering analyses here, since the breakup cross section is quite small even for scattering of ^{31}Ne with small neutron separation energy [20]. A microscopic optical potential U between a projectile (P) and a target (T) is constructed by folding the effective nucleon-nucleon (NN) interaction with the projectile and target densities ρ_P and ρ_T, respectively. The direct (U_{DR}) and exchange (U_{EX}) parts of the folding potential are obtained by [24,25]

$$U_{DR}(\boldsymbol{R}) = \int \rho_P(\boldsymbol{r}_P)\rho_T(\boldsymbol{r}_T)v_{DR}(\rho, \boldsymbol{s})d\boldsymbol{r}_P d\boldsymbol{r}_T, \quad (1)$$

$$U_{EX}(\boldsymbol{R}) = \int \rho_P(\boldsymbol{r}_P, \boldsymbol{r}_P - \boldsymbol{s})\rho_T(\boldsymbol{r}_T, \boldsymbol{r}_T + \boldsymbol{s})v_{EX}(\rho, \boldsymbol{s}) \times \exp[i\boldsymbol{K}(\boldsymbol{R}) \cdot \boldsymbol{s}/M]d\boldsymbol{r}_P d\boldsymbol{r}_T, \quad (2)$$

where $\boldsymbol{s} = \boldsymbol{r}_P - \boldsymbol{r}_T + \boldsymbol{R}$ for a position vector $\boldsymbol{R}$ of the center-of-mass (c.m.) of P from that of T. The original form of U_{EX} is a nonlocal function of $\boldsymbol{R}$, but it has been localized in Eq. (2) with the local semiclassical approximation [26], where $\hbar\boldsymbol{K}(\boldsymbol{R})$ is the local momentum of the scattering considered and $M = A_P A_T/(A_P + A_T)$ for the mass number A_P (A_T) of P (T). The validity of this localization is shown in Ref. [27] for nucleon-nucleus scattering; note that this is also the case with nucleus-nucleus scattering. In Eqs. (1) and (2), the direct (exchange) component of the effective NN interaction, v_{DR} (v_{EX}), is assumed to depend on the local density at the midpoint of the interacting nucleon pair. We adopt the Melbourne g matrix as an effective NN interaction in nuclear medium. The Schrödinger equation with $U_{DR} + U_{EX}$ is solved for each relative angular momentum (L) between P and T; see Ref. [22] for the details. The reaction cross section σ_R is obtained from the Lth component S_L of the scattering matrix as

$$\sigma_R = \frac{\pi}{K^2}\sum_L (2L + 1)(1 - |S_L|^2), \quad (3)$$

where K is the relative wave number.

The projectile densities ρ_P of $^{28-32}$Ne are calculated from the AMD wave functions that successfully describe the low-lying spectrum of Ne isotopes and free from the spurious c.m. motion; see Ref. [14] for the details. To investigate one-neutron-halo nature, we have performed a more sophisticated calculation for ^{31}Ne, which is called AMD-RGM below. By employing the coupled-channels RGM-type wave function

$$\Psi(^{31}\mathrm{Ne}; 3/2_1^-) = \sum_{nJ\pi} \mathcal{A}\{\chi_{nl}(r)Y_{lm}(\hat{\boldsymbol{r}})\Psi(^{30}\mathrm{Ne}; J_n^\pi)\phi_n\}, \quad (4)$$

the relative wave function χ_{nl} between the last neutron and the core (^{30}Ne) is calculated by solving the RGM equation. Here the wave functions of ^{30}Ne are those of the AMD obtained in Ref [14] and includes the many excited states with positive and negative parity below 10 MeV in excitation energy. Therefore, note that the weak-binding feature and the possible core excitation associated with the strong deformation are properly treated in the AMD-RGM calculation. As for ρ_T, we use the phenomenological ^{12}C density deduced from the electron scattering [28], with the finite-size effect of the proton charge unfolded following the standard manner [29].

If one or both of the densities ρ_P and ρ_T are nonspherical, the microscopic potential U is not spherical. It follows from Refs. [22,30], however, that it is sufficient to use an angular-averaged density in DFM, i.e., Eqs. (1) and (2), in the present case. Nevertheless, deformation effects of the wave functions are taken into account as shown in Ref. [22].

Results and discussions.—We show in Fig. 1 the result of σ_R for ^{12}C, ^{20}Ne, ^{23}Na, and ^{27}Al by a ^{12}C target at around 250 MeV/nucleon, compared with the experimental data [31–33]. For ^{20}Ne and ^{23}Na, the original experimental data were measured at around 950 MeV/nucleon [32,33], but the present ones are corrected in 240 MeV/nucleon by Glauber calculation [31]. The projectile densities are phenomenological ones obtained by electron scattering [28]. The theoretical results of σ_R shown in this Letter are reduced by 1.8% as in Ref. [22]. This fine-tuning has been done to reproduce the mean value of the σ_R of the ^{12}C-^{12}C scattering measured at 250.8 MeV/nucleon [31]. Thus, the present calculation contains no adjustable parameters except for the ^{12}C-^{12}C scattering. Figure 1 shows the high accuracy of the σ_R predicted by the present DFM calculation for the ^{20}Ne, ^{23}Na, and ^{27}Al projectiles.

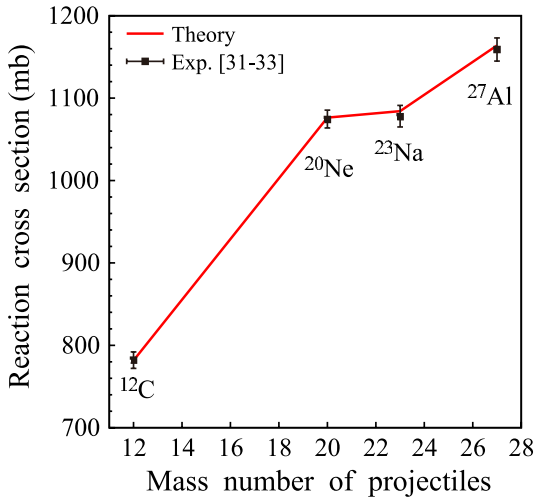

FIG. 1 (color online). Reaction cross sections for scattering of stable nuclei from ^{12}C at 250 MeV/nucleon. The solid line represents the results of the present double-folding model calculation. The experimental data are taken from Refs. [31–33].

TABLE I. The spin parity and deformation parameters β and γ of the ground states of Ne isotopes calculated by AMD.

Nuclide	^{28}Ne	^{29}Ne	^{30}Ne	^{31}Ne	^{32}Ne
J^π	0^+	$1/2^+$	0^+	$3/2^-$	0^+
β	0.28	0.43	0.39	0.41	0.33
γ	60°	0°	0°	0°	0°

The structural properties of $^{28-32}$Ne obtained by AMD are shown in Table I (spin parity and deformation parameters β and γ defined by the Hill-Wheeler coordinate) and Fig. 2 (one-neutron separation energies S_n). In the latter, experimental data [34,35] are also shown. One clearly sees that $^{28-32}$Ne are strongly deformed and the odd-even staggering of S_n measured is reproduced very well. It is thus expected that the AMD wave functions of Ne isotopes are highly reliable. However, for ^{31}Ne, which has very small S_n ($\sim$ 250 keV), the tail of the wave function of the last neutron may not be described properly, since AMD uses a one-range Gaussian wave function for the motion of each nucleon.

This possible shortcoming can be overcome by using RGM, which generates a proper asymptotics of the last neutron. The neutron one-body density $\rho_n(r)$ of ^{31}Ne thus obtained is shown in Fig. 3 by the solid line. The results for ^{31}Ne (dashed line) without RGM are also shown for comparison. The solid line has a long tail, whereas the dashed line rapidly falls off at $r \gtrsim 6$ fm. The root mean square radius of the density obtained by AMD-RGM (AMD) is 3.62 fm (3.49 fm). Although the difference between the two values is not so large, the density in the tail region, i.e., $r \gtrsim 6$ fm, has a significant contribution to σ_R as shown below. Note that AMD-RGM gives $S_n = 450$ keV, which is slightly larger than 250 keV obtained by AMD but still consistent with the measured value $S_n = 0.29 \pm 1.64$ MeV [34].

The AMD-RGM and AMD wave functions of ^{31}Ne can be decomposed in terms of the single-particle components as shown in Table II. Compared to AMD, the amount of 2^+ states reduces in AMD-RGM. This is due to the weak coupling between ^{30}Ne and valence neutron. In AMD-RGM, the main component of the last neutron is $1p_{3/2}$ coupled with the 0^+ ground state of ^{30}Ne. The long range tail of $\rho_n(r)$, i.e., the halo structure, shown in Fig. 3 is due to this configuration of ^{31}Ne.

Recently, the amount of the $1p_{3/2}$ component was estimated from the measured σ_{-n} with the spherical potential model [18]. In the analysis, the deformation was not considered, and the one-neutron separation energy was assumed to be identical with the single-particle energy. Justification of this treatment of the ^{31}Ne wave function will be necessary for a quantitative comparison between the results in the present study and Ref. [18]. Note that we obtain the S_n and the spectroscopic amplitude microscopically, so we cannot change these values independently or freely.

Figure 4 shows σ_R of $^{28-32}$Ne by ^{12}C scattering at 240 MeV/nucleon. AMD (solid line) yields excellent agreement with the data for $^{28-30,32}$Ne. For ^{31}Ne, AMD-RGM (triangle) reproduces the data, whereas AMD does not. The tail correction to the projectile density is significant for ^{31}Ne. The spherical HF calculations (dotted line) significantly undershoot the data; here the c.m. correction [36] is made to the densities. More seriously, no bound-state solution is found for ^{31,32}Ne. We thus conclude that (i) $^{28-32}$Ne are strongly deformed as discussed in Ref. [22] and (ii) ^{31}Ne has a halo structure due to the last neutron in the $1p_{3/2}$ orbit.

In our previous work [22], σ_R was calculated by the deformed WS model with the β evaluated by AMD, but the

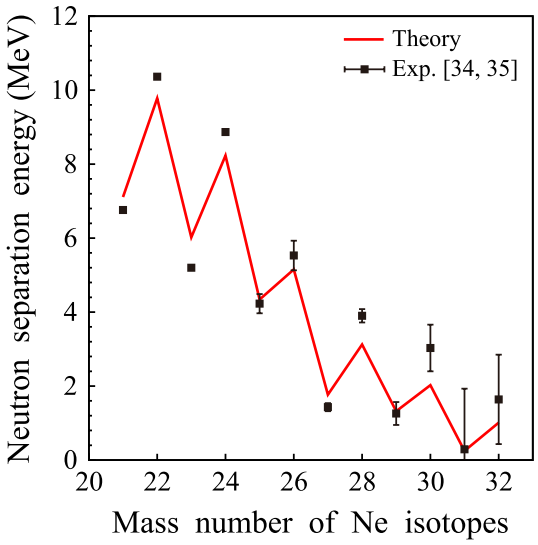

FIG. 2 (color online). One-neutron separation energy S_n of the Ne isotopes. The experimental data are taken from Refs. [34,35].

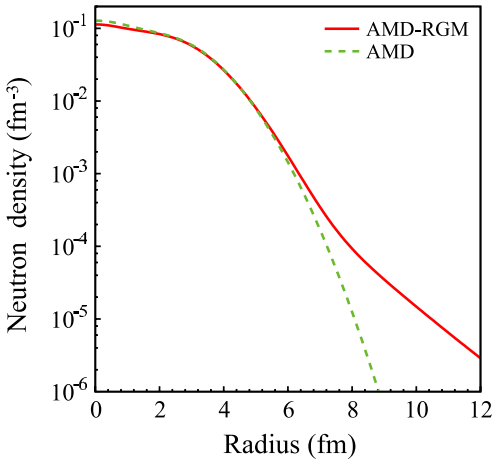

FIG. 3 (color online). The neutron one-body densities of ^{31}Ne. The solid and dashed lines represent the results of ^{31}Ne calculated by AMD-RGM and AMD, respectively.

TABLE II. Configurations of the ground state of ^{31}Ne obtained by AMD-RGM and AMD.

Configurations	Amplitude AMD-RGM	AMD
$^{30}\mathrm{Ne}(0^+) \otimes 1p_{3/2}$	56%	37%
$^{30}\mathrm{Ne}(2^+) \otimes 1p_{3/2}$	24%	41%
$^{30}\mathrm{Ne}(2^+) \otimes 0f_{7/2}$	9%	12%
$^{30}\mathrm{Ne}(1^-) \otimes 1s_{1/2}$	5%	5%
Other components	6%	5%

c.m. correction was not made to the densities. After making the correction, the result (dashed line) almost agrees with the AMD result for $^{28-29}$Ne and the AMD-RGM result for ^{31}Ne. For ^{30,32}Ne, the deformed WS model overshoots the AMD results by about 20 mb, but the results of the deformed WS model are still consistent with the data.

Very recently, the pairing antihalo effect was discussed for odd-even staggering of σ_R for $^{30-32}$Ne [37]. It will be interesting to consider the pairing effect in the present framework. It will be quite interesting how the strong deformation indicated by AMD affects the result of Ref. [37].

Summary.—We have performed a microscopic calculation of the reaction cross sections for neutron-rich Ne isotopes systematically. The DFM with the Melbourne g matrix and the AMD wave functions were used. AMD is a powerful tool that describes strongly deformed nuclei. For a loosely bound nucleus ^{31}Ne, the RGM was adopted to generate a proper behavior of the wave function of the last neutron. The present framework reproduced the experimental data very well with no free adjustable parameters. Therefore, the AMD wave functions of the Ne isotopes (AMD-RGM for ^{31}Ne) were clearly validated. We thus concluded that neutron-rich Ne isotopes are strongly deformed and ^{31}Ne has a halo structure with spin parity $3/2^-$.

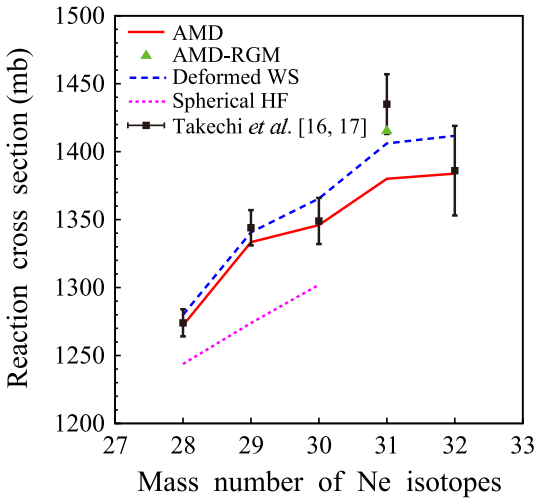

FIG. 4 (color online). Reaction cross sections of Ne isotopes by ^{12}C at 240 MeV/nucleon. The solid line represents the AMD result, whereas the triangle does the AMD-RGM result for ^{31}Ne. The dashed line shows the result of the deformed WS model in Ref. [22]. The dotted line corresponds to the result of the spherical HF. The experimental data are taken from Refs. [16,17].

The authors thank M. Takechi for providing the values of the experimental data and H. Sakurai and M. Fukuda for useful discussions. This work is supported in part by Grants-in-Aid for Scientific Research (C) No. 22540285 and No. 22740169 from Japan Society for the Promotion of Science. The numerical calculations of this work were performed on the computing system in Research Institute for Information Technology of Kyushu University.

[1] E. K. Warburton, J. A. Becker, and B. A. Brown, Phys. Rev. C **41**, 1147 (1990).
[2] N. Fukunishi, T. Otsuka, and T. Sebe, Phys. Lett. B **296**, 279 (1992).
[3] T. Motobayashi *et al.*, Phys. Lett. B **346**, 9 (1995).
[4] E. Caurier, F. Nowacki, A. Poves, and J. Retamosa, Phys. Rev. C **58**, 2033 (1998).
[5] Y. Utsuno, T. Otsuka, T. Mizusaki, and M. Honma, Phys. Rev. C **60**, 054315 (1999).
[6] H. Iwasaki *et al.*, Phys. Lett. B **522**, 227 (2001).
[7] Y. Yanagisawa *et al.*, Phys. Lett. B **566**, 84 (2003).
[8] A. Poves and J. Retamosa, Nucl. Phys. **A571**, 221 (1994).
[9] P. Descouvemont, Nucl. Phys. **A655**, 440 (1999).
[10] J. Terasaki, H. Flocard, P.-H. Heenen, and P. Bonche, Nucl. Phys. **A621**, 706 (1997).
[11] R. Rodríguez-Guzmán, J. L. Egido, and L. M. Robledo, Nucl. Phys. **A709**, 201 (2002).
[12] M. Yamagami and Nguyen Van Giai, Phys. Rev. C **69**, 034301 (2004).
[13] R. R. Rodríguez-Guzmán, J. L. Egido, and L. M. Robledo, Eur. Phys. J. A **17**, 37 (2003).
[14] M. Kimura and H. Horiuchi, Prog. Theor. Phys. **111**, 841 (2004); M. Kimura, Phys. Rev. C **75**, 041302 (2007); arXiv:1105.3281.
[15] T. Nakamura *et al.*, Phys. Rev. Lett. **103**, 262501 (2009).
[16] M. Takechi *et al.*, Nucl. Phys. **A834**, 412c (2010).
[17] M. Takechi *et al.*, Mod. Phys. Lett. A **25**, 1878 (2010).
[18] W. Horiuchi, Y. Suzuki, P. Capel, and D. Baye, Phys. Rev. C **81**, 024606 (2010).
[19] Y. Urata, K. Hagino, and H. Sagawa, Phys. Rev. C **83**, 041303(R) (2011).
[20] M. Yahiro, K. Ogata, and K. Minomo, Prog. Theor. Phys. **126**, 167 (2011).
[21] P. Capel, W. Horiuchi, Y. Suzuki, and D. Baye, Mod. Phys. Lett. A **25**, 1882 (2010).
[22] K. Minomo, T. Sumi, M. Kimura, K. Ogata, Y. R. Shimizu, and M. Yahiro, Phys. Rev. C **84**, 034602 (2011).
[23] K. Amos, P. J. Dortmans, H. V. von Geramb, S. Karataglidis, and J. Raynal, Adv. Nucl. Phys. **25**, 275 (2000).
[24] B. Sinha, Phys. Rep. **20**, 1 (1975); B. Sinha and S. A. Moszkowski, Phys. Lett. **81B**, 289 (1979).

[25] T. Furumoto, Y. Sakuragi, and Y. Yamamoto, Phys. Rev. C **82**, 044612 (2010).
[26] F. A. Brieva and J. R. Rook, Nucl. Phys. **A291**, 299 (1977); **A291**, 317 (1977); **A297**, 206 (1978).
[27] K. Minomo, K. Ogata, M. Kohno, Y. R. Shimizu, and M. Yahiro, J. Phys. G **37**, 085011 (2010).
[28] H. de Vries, C. W. de Jager, and C. de Vries, At. Data Nucl. Data Tables **36**, 495 (1987).
[29] R. P. Singhal *et al.*, Nucl. Instrum. Methods **148**, 113 (1978).
[30] G. R. Satchler and W. G. Love, Phys. Rep. **55**, 183 (1979).
[31] M. Takechi *et al.*, Phys. Rev. C **79**, 061601(R) (2009).
[32] L. Chulkov *et al.*, Nucl. Phys. **A603**, 219 (1996).
[33] T. Suzuki *et al.*, Phys. Rev. Lett. **75**, 3241 (1995).
[34] B. Jurado *et al.*, Phys. Lett. B **649**, 43 (2007).
[35] G. Audi, A. H. Wapstra, and C. Thibault, Nucl. Phys. **A729**, 337 (2003).
[36] L. J. Tassie and F. C. Barker, Phys. Rev. **111**, 940 (1958).
[37] K. Hagino and H. Sagawa, Phys. Rev. C **84**, 011303(R) (2011).